

UC Berkeley

UC Berkeley Previously Published Works

Title

Direct measurements of the convective recycling of the upper troposphere.

Permalink

<https://escholarship.org/uc/item/8g16x57g>

Journal

Science (New York, N.Y.), 315(5813)

ISSN

0036-8075

Authors

Bertram, Timothy H
Perring, Anne E
Wooldridge, Paul J
et al.

Publication Date

2007-02-01

DOI

10.1126/science.1134548

Copyright Information

This work is made available under the terms of a Creative Commons Attribution License, available at <https://creativecommons.org/licenses/by/4.0/>

Peer reviewed

Direct Measurements of the Convective Recycling of the Upper Troposphere

Timothy H. Bertram,¹ Anne E. Perring,¹ Paul J. Wooldridge,¹ John D. Crounse,² Alan J. Kwan,³ Paul O. Wennberg,^{3,4} Eric Scheuer,⁵ Jack Dibb,⁵ Melody Avery,⁶ Glen Sachse,⁶ Stephanie A. Vay,⁶ James H. Crawford,⁶ Cameron S. McNaughton,⁷ Antony Clarke,⁷ Kenneth E. Pickering,^{8,9} Henry Fuelberg,¹⁰ Greg Huey,¹¹ Donald R. Blake,¹² Hanwant B. Singh,¹³ Samuel R. Hall,¹⁴ Richard E. Shetter,¹⁴ Alan Fried,¹⁴ Brian G. Heikes,¹⁵ Ronald C. Cohen^{1,16*}

We present a statistical representation of the aggregate effects of deep convection on the chemistry and dynamics of the upper troposphere (UT) based on direct aircraft observations of the chemical composition of the UT over the eastern United States and Canada during summer. These measurements provide unique observational constraints on the chemistry occurring downwind of convection and the rate at which air in the UT is recycled. These results provide quantitative measures that can be used to evaluate global climate and chemistry models.

Deep convection is a highly efficient mechanism for the vertical transport of air from near Earth's surface (0 to 2 km) to the UT (6 to 12 km) (1–5). Typical convective storms have spatial scales of tens of kilometers and vertical velocities as large as 15 m s^{-1} (6), making their local influence in the UT extremely strong. The rapid upward flow is balanced by downdrafts within the convective storms and much slower descending flow that occurs over a larger spatial scale (7). Convection is also associated with lightning, an important source of NO_x ($\text{NO}_x \equiv \text{NO} + \text{NO}_2$) in the UT (8, 9). The source strength and spatial distribution of lightning NO_x emissions are not well known, with estimates ranging from 2 to $20 \text{ Tg N year}^{-1}$ for the global average (10), compared to 25 Tg

N year^{-1} from fossil fuel combustion (11). Although there have been a number of case studies of the chemical effects of individual storms (12), studies of the aggregate effects of convection on the chemical composition and radiative forcing of the UT have been largely the province of modeling and theory (13, 14). Here, we describe measurements that provide a direct link between an observable property and the ensemble of convective events.

The chemical and radiative consequences of convection and lightning are known to be large (2, 15, 16). Upper tropospheric O_3 , either transported directly from the boundary layer via convection or formed in situ after detrainment of convectively lofted O_3 precursors [NO_x , odd hydrogen radicals (HO_x), and hydrocarbons] in the outflow region, directly affects climate through a positive radiative forcing (15). Additionally, deep convection accounts for a substantial fraction of the net flux of moisture from near Earth's surface to the UT (17) (Fig. 1). Thus, the rate at which the UT is turned over by convection

has important implications for the hydrological cycle and the magnitude of the water vapor feedback on global temperature (18).

We describe a method for calculating, from in situ measurements of the chemical composition of the UT, the length of time that an air mass spends in the UT after convection, and we discuss the chemistry occurring in the outflow region as a function of time since convection. We use measurements of NO_2 (19, 20) (NO_x is calculated from NO_2 , O_3 , HO_2 , and photolysis rates), HNO_3 (21, 22), OH and HO_2 (23), O_3 , aerosol number density (24), SO_2 , actinic flux [from which photolysis rate coefficients (J_x) for NO_2 (J_{NO_2}), HNO_3 (J_{HNO_3}), and many other species are calculated] (25), CO (26), and CO_2 (27) obtained during the Intercontinental Chemical Transport Experiment–North America (INTEX-NA) aboard the NASA DC-8 (28). Measurements were made at altitudes between the surface and 12.5 km over a wide area of the United States and Canada, west of 40°W and between 30° and 50°N . There were a large number of vertical profiles, allowing a reasonably unbiased statistical sampling of air over this region during July and August 2004.

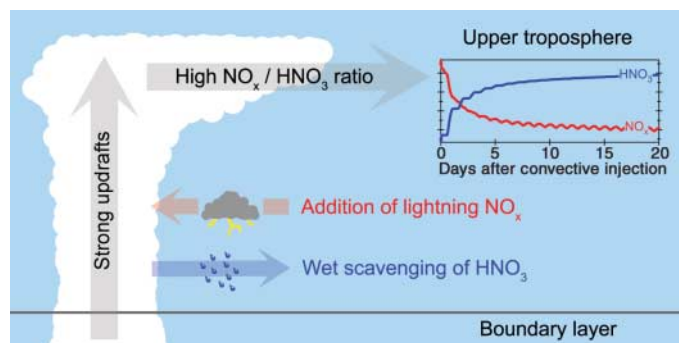
We use the deviation of the observed NO_x/HNO_3 ratio from steady state as an indicator of convective influence. The NO_x/HNO_3 ratio is reset to near infinity in moist convection as a result of preferential wet scavenging of HNO_3 relative to NO_x (i.e., the solubility of HNO_3 is $\sim 10^8$ times that of NO_x) (29). Further, lightning-produced NO_x , often coincident with convection, markedly enhances NO_x in the outflow region. The coupling of these processes makes the NO_x/HNO_3 ratio in the UT an effective indicator of convective influence, where $\text{NO}_x/\text{HNO}_3 \gg 1$ is indicative of recent cloud outflow (30, 31). In the days after convection, the ratio decays toward steady state, providing a chemical clock that marks the length of time that an air mass has spent in the UT after convection (32). Previous studies have used species that have no UT source (e.g., CH_3I) (33) or alternative chemical ratios to provide estimates of age of air in the UT (34, 35). Our study is unique because of the availability of

¹Department of Chemistry, University of California, Berkeley, CA 94720, USA. ²Division of Chemistry and Chemical Engineering, California Institute of Technology, Pasadena, CA 91125, USA. ³Division of Engineering and Applied Science, California Institute of Technology, Pasadena, CA 91125, USA. ⁴Division of Geological and Planetary Sciences, California Institute of Technology, Pasadena, CA 91125, USA. ⁵Institute for the Study of Earth, Oceans, and Space, University of New Hampshire, Durham, NH 03824, USA. ⁶NASA Langley Research Center, Hampton, VA 23681, USA. ⁷School of Ocean and Earth Science Technology, University of Hawaii at Manoa, Honolulu, HI 96822, USA. ⁸Department of Atmospheric and Oceanic Science, University of Maryland, College Park, MD 20742, USA. ⁹NASA Goddard Space Flight Center, Greenbelt, MD 20771, USA. ¹⁰Department of Meteorology, Florida State University, Tallahassee, FL 32306, USA. ¹¹School of Earth and Atmospheric Sciences, Georgia Institute of Technology, Atlanta, GA 30332, USA. ¹²Department of Chemistry, University of California, Irvine, CA 92697, USA. ¹³NASA Ames Research Center, Moffett Field, CA 94035, USA. ¹⁴National Center for Atmospheric Research, Boulder, CO 80305, USA. ¹⁵Graduate School of Oceanography, University of Rhode Island, Narragansett, RI 02882, USA. ¹⁶Department of Earth and Planetary Science, University of California, Berkeley, CA 94720, USA.

*To whom correspondence should be addressed. E-mail: cohen@cchem.berkeley.edu

Fig. 1. In moist convection, air from near Earth's surface is rapidly transported upward and detrained into the UT. In this process, nitric acid (highly soluble) is efficiently scavenged while NO_x (insoluble) remains. NO_x is elevated by concurrent lightning NO production, resulting in high NO_x/HNO_3 ratios in the convective outflow region.

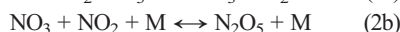
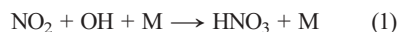
After detrainment into the UT, NO_x is converted to HNO_3 by OH during the day and through reaction with NO_3 , followed by hydrolysis of the N_2O_5 product, at night. The chemical evolution of the NO_x/HNO_3 ratio provides a unique indicator of the length of time that a sampled air mass has been in the UT after convection.



NO_2 , OH, and HNO_3 measurements with high time resolution, which allows us to build a much more extensive data set than in previous studies. After the initial turbulent mixing in the near field of the convection, mixing is slow; thus, the time evolution of the NO_x/HNO_3 ratio after convection depends largely on the partitioning of NO_x (between NO and NO_2), the concentration of OH, and the actinic flux.

Reactive nitrogen partitioning in the UT.

The chemical sinks of UT NO_x are reaction with OH to produce HNO_3 (Eq. 1) and loss through NO_3 (Eqs. 2a and 2b), where M represents a third molecule (e.g., N_2 , O_2) that absorbs the excess vibrational energy of the association reaction, followed by hydrolysis of N_2O_5 to produce HNO_3 (36). NO_x is regenerated by HNO_3 photolysis and reaction of OH with HNO_3 (and subsequent NO_3 photolysis to NO_2) (Eqs. 3 and 4).



Assuming a diurnal steady state for HNO_3 , the NO_x/HNO_3 ratio can be calculated as

$$\frac{\left(\frac{[\text{NO}_x]}{[\text{HNO}_3]} \right)_{\text{steady-state}}}{J_{\text{HNO}_3} + k_{\text{HNO}_3+\text{OH}}[\text{OH}]} = \frac{k_{\text{NO}_2+\text{OH}}[\text{OH}] + 2k_{\text{N}_2\text{O}_5+\text{H}_2\text{O}} \frac{[\text{N}_2\text{O}_5]}{[\text{NO}_2]}}{\left(\frac{[\text{NO}_2]}{[\text{NO}_x]} \right)} \times \left(\frac{[\text{NO}_2]}{[\text{NO}_x]} \right) \quad (5)$$

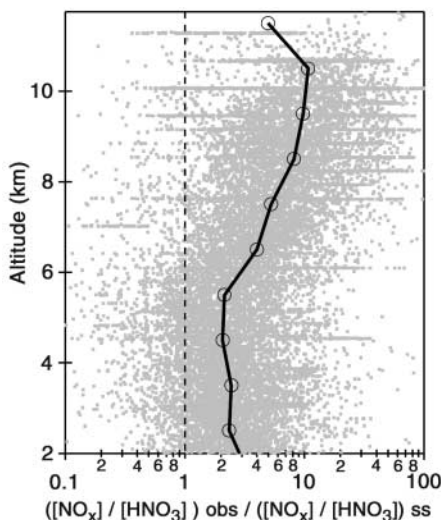


Fig. 2. Observed deviation of the NO_x/HNO_3 ratio from steady state as a function of altitude in the UT. The mean values within 1-km vertical bins are denoted by circles. The steady-state NO_x/HNO_3 ratio was calculated from measured NO_x , OH, and J_{HNO_3} . The grayscale data points were calculated from all observations taken during INTEX-NA.

where k is the reaction rate coefficient. NO_x/HNO_3 is expected to be larger than the steady-state value because wet scavenging removes HNO_3 faster than the time to reach steady state (37). Our observations show the NO_x/HNO_3 ratio to be much higher than the ratio described by Eq. 5 at altitudes greater than 6 km (Fig. 2). The difference between the observed ratio and that predicted by Eq. 5 grows with altitude, reaching a maximum at 10 km. Previous observations of NO_x and HNO_3 [either measured directly or calculated from observations of NO_x , peroxyacetyl nitrate (PAN), and $\text{NO}_y \equiv \text{NO}_x + \text{total peroxy nitrates} + \text{total alkyl nitrates} + \text{HNO}_3 + 2 \times \text{N}_2\text{O}_5 + \text{other minor components}$] have shown NO_x/HNO_3 to be significantly larger than the steady-state prediction in the UT (30, 31, 38–42). This has been shown to be primarily a result of convection and lightning reinitializing the system before steady state is achieved (30, 31). Although there are other hypotheses (40–42), we [like Jaeglé *et al.* (31)] find no evidence for a mechanism other than convection responsible for holding NO_x/HNO_3 out of steady state in the UT.

Chemical signatures of convection. Figure 3 depicts one of many convectively influenced air masses sampled in the UT during INTEX-NA. Three distinct convective events (40 to 80 km wide) are identified by enhancements in NO_x/HNO_3 in Fig. 3A. Coincident enhancements are present in SO_2 , an indicator of a recent boundary-layer source for this air, and in ultrafine condensation nuclei (UCN) ($3 \leq D_p \leq 10$ nm, where D_p is the particle diameter), an indicator of cloud detrainment (Fig. 3B) (43, 44). Sharp decreases in CO_2 also indicate the presence of boundary-layer air that has been depleted in CO_2 by photosynthetic activity (Fig. 3C) (44). Enhancements in CO, CH_2O , and various hydrocarbons relative to the surrounding UT air were also observed in these plumes, confirming that these parcels originate from the planetary boundary layer (PBL). Backward air trajectories, initialized along the flight track and mapped onto the spatial and temporal distribution of cloud-to-ground lightning strikes, indicate that this air mass was influenced by lightning about 1 day before DC-8 sampling (Fig. 3E). Such features with high NO_x/HNO_3 ratios were observed throughout the UT during INTEX-NA.

To assess the extent to which the UT over the eastern United States and Canada during the summer of 2004 was influenced by convection, and to describe the chemical evolution of convective outflow, we used a constrained time-dependent photochemical box model to map the observed NO_x/HNO_3 ratio to the time since the ratio was last reinitialized (45). It was initialized with observations at 1-km vertical intervals from 6 to 12 km. The derived timing indicator for the convectively influenced air sampled on 11 August 2006 is shown in Fig. 3D. The properties of the ensemble of our measurements are shown in Figs. 4 to 6.

The aerosol size distribution provides an independent indicator of air recently detrained from clouds. Cloud-processed air is depleted of aerosol surface area, permitting new particle formation in the outflow region (43, 44). Figure 4A depicts the fraction of condensation nuclei found in the 3- to 10-nm bin as a function of time since convective influence. The fraction of particles in this ultrafine mode is largest during the first few days, which confirms that the NO_x/HNO_3 ratio, and the timing indicator derived from it, is reinitialized in the UT by cloud processing. Strong enhancements in $\text{CH}_3\text{OOH}/\text{H}_2\text{O}_2$, also an indicator of recent cloud processing (33), were observed during the first 2 days after cloud processing.

As expected, both elevated NO_x and suppressed HNO_3 are observed at short times (Fig. 4, B and C). Enhancement in NO_x during the first few days is indicative of convection of boundary-layer and/or lightning NO_x (46). The suppression of HNO_3 at short times is clear indication of HNO_3 scavenging during convection. Figure 4D confirms that reactive nitrogen (NO_y) is conserved during the chemical processing after convection, a fact that provides further support for the use of NO_x/HNO_3 as a marker representing time since convection.

Chemical processing in convective outflow.

Mapping the ensemble of observations made throughout the UT onto the coordinate of time since convection allows us to assess the chemical and dynamical processes occurring after convection without attempting a Lagrangian convection study. In this analysis we concentrate on the time evolution of CO and O_3 .

The time evolution of CO after detrainment into the UT is set by the abundance of OH and the rate at which the convective plume entrains air from the background UT (Fig. 5A). Because the chemical clock directly depends on HO_x , we constrained both OH and HO_2 to the observations as a function of NO_x and pressure in the time-dependent model used to generate time. As a result, we can iterate the model to determine the proper mixing rate of the convective plume by matching the modeled and observed time evolution of CO after convection. Using this approach for a series of long-lived species (e.g., CO, CH_4 , CH_3OH), we calculated an average mixing rate of $0.05 \pm 0.02 \text{ day}^{-1}$ after detrainment into the UT. This is in good agreement with the upper limit of 0.06 to 0.1 day^{-1} determined by Ray *et al.* from observations of convective plumes observed in the stratosphere (47). However, it is slower than the 2-day dilution time scale determined by Wang *et al.* from observations in the UT (32). Because the DC-8 did not routinely sample in the turbulent environment directly surrounding convective outflow, this mixing rate likely reflects diffusive and shear-induced mixing subsequent to the initial turbulent mixing occurring during detrainment from the convective system.

Figure 5B shows the O_3 mixing ratio as a function of time since convection. We find that

on average, convectively lofted air masses contain less O_3 than the background UT. This result is consistent with the observed vertical gradient in O_3 measured over the continental United States during INTEX-NA, with lower O_3 in the PBL than above (48). Rapid changes in the O_3 mixing ratio are observed during the first 2 days after detrainment, with the observed O_3 10 nmol mol^{-1} above the initial value by the end of day 2. The observed rate of increase slows exponentially with an asymptote at long times approaching zero and the O_3 mixing ratio approaching a constant value of 82 nmol mol^{-1} . This is a surprising result, as our model of the O_3 rate of change never approaches zero but continues to predict a net increase of $3 \text{ nmol mol}^{-1} \text{ O}_3 \text{ day}^{-1}$ at the end of day 5 (49).

Constraints on the convective turnover rate of the UT. The convective turnover rate of the UT is critical for accurately describing NO_x , HO_x , and O_3 chemistry in the UT (50). However, at present there are few observation-based constraints available (either meteorological or chemical) to test the aggregate effects of convection in the current generation of global chemistry and climate models. To determine the convective turnover rate of the UT from the observations

presented here, it is necessary to know with high confidence both the extent to which the UT is influenced by convection and the fraction of PBL air in the convectively influenced air masses.

To determine the fraction of PBL air contained in fresh convective outflow, we used observations of insoluble long-lived species. Assuming that we conducted a statistically unbiased sampling of both the boundary layer and free troposphere during INTEX-NA, we can calculate the fraction of PBL air present in fresh convection (f) according to

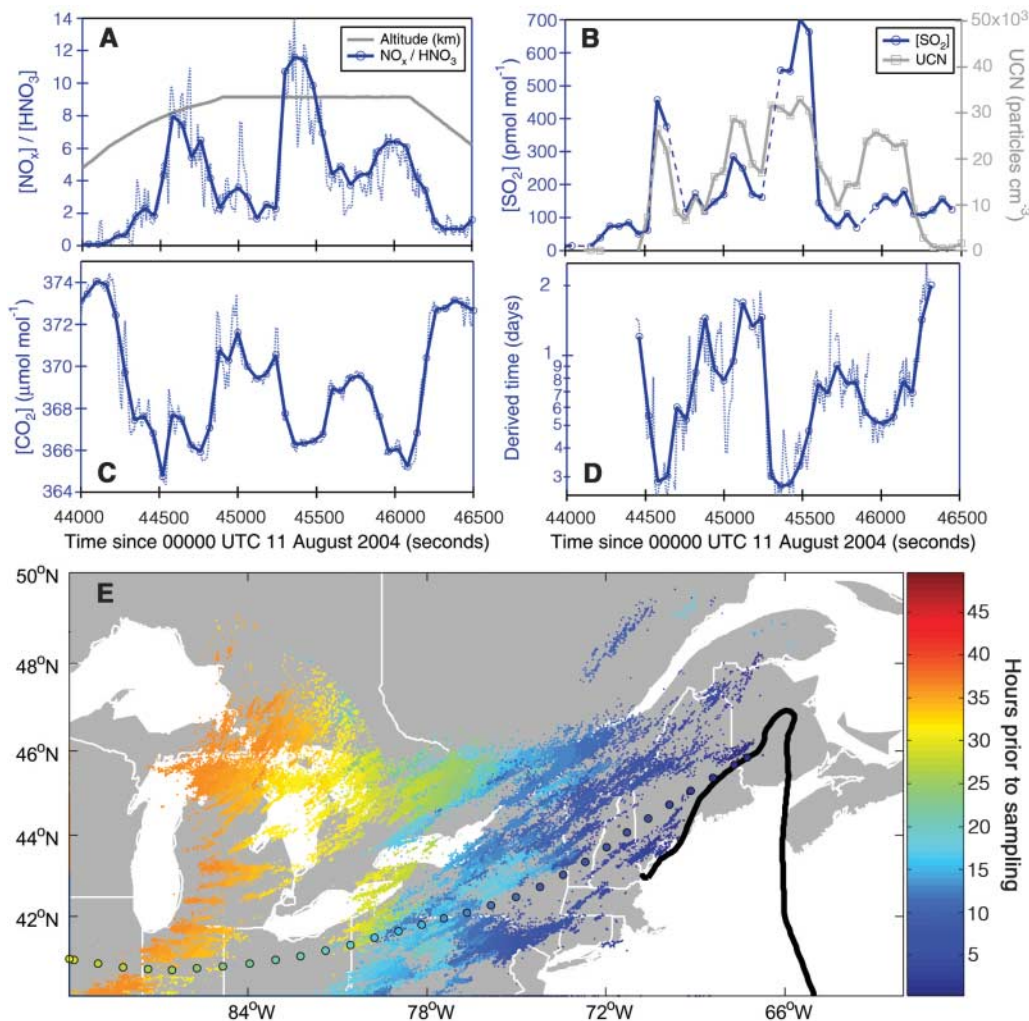
$$[X]_{\text{UT}(t=0)} = f[X]_{\text{surface}} + (1-f)[X]_{\text{UT}} \quad (6)$$

where $[X]_{\text{UT}(t=0)}$ is the mean mixing ratio of species X in fresh convective outflow (as identified using our timing indicator), $[X]_{\text{UT}}$ is the mean mixing ratio of species X in the UT (7.5 to 11.5 km), and $[X]_{\text{surface}}$ is the mean mixing ratio of species X between 0 and 1.5 km. Using observations of CO , CO_2 , CH_3OH , CH_4 , and C_2H_6 we calculated the fraction of PBL air in fresh convection to be 0.19 ± 0.05 , 0.11 ± 0.03 , 0.26 ± 0.05 , 0.15 ± 0.05 , and 0.34 ± 0.09 , respectively. We calculated a weighted average

for the fraction of PBL air in convective outflow of 0.17 ± 0.02 by weighting each value by the inverse square of its uncertainty. This result implies that convectively lofted PBL air rapidly entrains the surrounding air either during ascent or in the turbulent environment of the detraining flow. These results are consistent with the observations of Ray *et al.*, who determined the fraction of tropospheric air in convective plumes sampled in the stratosphere to be between 0.1 and 0.4 (47). However, our results suggest a smaller fraction than the observations of Cohan *et al.*, who calculated the fraction of boundary-layer air in fresh convective outflow to be between 0.32 and 0.64 (33), and the modeling studies of Mullendore *et al.*, who calculated the fraction of PBL air present in the convective outflow region of a supercell storm 10 hours after storm initialization to be 0.26 (51).

Figure 6A shows the normalized frequency distribution of the time since convection, based on the NO_x/HNO_3 ratio. We found that 54% of the air between 7.5 and 11.5 km was influenced by convection during the past 2 days. The convective outflow was strongest between 9.5 and 10.5 km, where the fraction of air that is less than 2 days old exceeds 69%. The vertical dis-

Fig. 3. (A to D) Time series of measurements taken in the vicinity of recent convective activity on 11 August 2004 between 5 and 9 km. (A) Three distinct convective plumes, each indicated by a sharp increase in the NO_x/HNO_3 ratio. (B and C) Coincident enhancements in SO_2 and UCN ($3 \text{ nm} > D_p > 10 \text{ nm}$) and coincident sharp drops in CO_2 , indicative of the convective lofting of boundary-layer air depleted in CO_2 . The derived time since the sampled air mass had been influenced by convection is shown in (D). (E) NLDN lightning hits (small dots) on 10 and 11 August. The color scale represents the time of the hit (hours) before aircraft sampling. The DC-8 sampling location corresponding to measurements shown in the top panel is located on the Maine–New Brunswick border (46°N , 67°W). The 2-day back-trajectory [initialized at the point of the second convective plume shown in (A)] is also color-coded by time before DC-8 sampling (circles with black edges). The DC-8 flight track on 11 August 2004 is shown by the heavy black line.



tribution presented here is consistent with previous analyses of convective outflow to the UT from individual storms (4, 52) and the vertical distribution of convectively influenced laminae observed in O_3 sonde data from the summer of 2004 over the northeastern United States. The shift toward longer times between 10.5 and 11.5 km suggests two possibilities: that convective cloud tops on average do not extend higher than 10.5 km over the mid-latitudes during summer (53), or that transport of stratospheric air rich in HNO_3 contributes to keeping the NO_x/HNO_3 ratio low at altitudes higher than 10.5 km.

To constrain the turnover rate of the UT from the ensemble statistics generated from our calculated time since convective influence (Fig. 6A), we constructed a two-dimensional (2D) model of the UT. On the basis of typical wind speeds, we assume that it takes 4 days for any individual model point to pass through the sampling region and that each point has not been influenced by

convection upon entering the sampling window. Every 6 hours, we represented convection by randomly reinitializing the age of $x\%$ of the points to 0 [the value of x is determined by the turnover rate (varied between 0.05 and 0.2 day^{-1}) and the fraction of PBL air contained in fresh convection (assumed to be a constant at 0.17)], and we then diluted each point with the mean value of the adjacent 8 points at the rate of 0.05 day^{-1} .

Figure 6B depicts the observed and three calculated normalized frequency distributions of time since convective influence between 7.5 and 11.5 km. The shape of the distribution suggests that UT air sampled during INTEX-NA was strongly influenced by convection, and that convectively lofted plumes did not have sufficient time to either mix or age before sampling; instead, air was transported to the east out of the domain. Calculated frequency distributions of time since convection, obtained by collecting the points in the eastern half of the 2D UT model analysis (where we sampled most frequently), are also shown in Fig. 6B. Assuming the DC-8 made a statistically unbiased sampling of the continental UT during summer, the best match among the three model calculations and observations would imply a convective turnover rate between 0.1 and 0.2 day^{-1} . However, if we assume that the DC-8 had a positive bias toward sampling fresh convection, our observed frequency distributions are most consistent with a convective turnover rate closer to 0.1 day^{-1} (54).

For comparison, the Goddard Earth Observing System (GEOS-4) data assimilation model detrainment cloud mass flux between 400 and 200 hPa (~ 7.2 to 11.8 km) for the domain (80° to 100°W for 30° to 35°N and 70° to 100°W for 35° to 50°N) between 1 July and 15 August

2004 was $0.0085 \text{ kg m}^{-2} \text{ s}^{-1}$. This corresponds to a turnover rate of 0.37 day^{-1} (using a column mass of $1.9 \times 10^3 \text{ kg m}^{-2}$ between 7.2 and 11.8 km). Further investigation is needed to understand the source of the difference between our observed turnover rate and the one derived from the model.

Conclusions. Our observations provide unique constraints on (i) the extent to which convection perturbs the continental UT during summer, (ii) the fraction of boundary-layer air present in convective outflow, and (iii) the convective overturning rate of the UT. In addition, the chemical clock described here defines a coordinate that can be used to assess the chemistry occurring downwind of convective injection. These direct measures of atmospheric rates present a new opportunity for quantitative tests of model representations of processes governing UT ozone, convection, and lightning and their impact on climate.

References and Notes

1. R. B. Chatfield, P. J. Crutzen, *J. Geophys. Res.* **89**, 7111 (1984).
2. R. R. Dickerson *et al.*, *Science* **235**, 460 (1987).
3. K. E. Pickering, R. R. Dickerson, G. J. Huffman, J. F. Boatman, A. Schanot, *J. Geophys. Res.* **93**, 759 (1988).
4. A. M. Thompson *et al.*, *J. Geophys. Res.* **99**, 18703 (1994).
5. W. J. Collins, R. G. Derwent, C. E. Johnson, D. S. Stevenson, *Q. J. R. Meteorol. Soc.* **128**, 991 (2002).
6. J. E. Dye *et al.*, *J. Geophys. Res.* **105**, 10023 (2000).
7. S. A. Rutledge, R. A. Houze, M. I. Biggerstaff, T. Matejka, *Mon. Weather Rev.* **116**, 1409 (1988).
8. H. Huntrieser, H. Schlager, C. Feigl, H. Holler, *J. Geophys. Res.* **103**, 28247 (1998).
9. B. Ridley *et al.*, *J. Geophys. Res.* **109**, D17305 (2004).
10. *Scientific Assessment of Ozone Depletion* World Meteorological Organization, Geneva, 1995.
11. L. Jaeglé, L. Steinberger, R. V. Martin, K. Chance, *Faraday Discuss.* **130**, 407 (2005).
12. A. J. DeCaria, K. E. Pickering, G. L. Stenchikov, L. E. Ott, *J. Geophys. Res.* **110**, D14303 (2005).
13. J. Lelieveld, P. J. Crutzen, *Science* **264**, 1759 (1994).
14. M. G. Lawrence, R. von Kuhlmann, M. Salzmann, P. J. Rasch, *Geophys. Res. Lett.* **30**, 10.1029/2003GL017644 (2003).
15. M. Gauss *et al.*, *J. Geophys. Res.* **108**, 10.1029/2002JD002624 (2003).
16. K. E. Pickering *et al.*, *J. Geophys. Res.* **95**, 14049 (1990).
17. I. Folkins, K. K. Kelly, E. M. Weinstock, *J. Geophys. Res.* **107**, 10.1029/2002JD002185 (2002).
18. M. T. Chahine, *Nature* **359**, 373 (1992).
19. J. A. Thornton, P. J. Wooldridge, R. C. Cohen, *Anal. Chem.* **72**, 528 (2000).
20. P. A. Cleary, P. J. Wooldridge, R. C. Cohen, *Appl. Opt.* **41**, 6950 (2002).
21. R. W. Talbot *et al.*, *Geophys. Res. Lett.* **26**, 3057 (1999).
22. J. D. Crounse, K. A. McKinney, A. J. Kwan, P. O. Wennberg, *Anal. Chem.* **78**, 6726 (2006).
23. I. C. Faloona *et al.*, *J. Atmos. Chem.* **47**, 139 (2004).
24. A. D. Clarke *et al.*, *J. Geophys. Res.* **109**, D15509 (2004).
25. R. E. Shetter, M. Müller, *J. Geophys. Res.* **104**, 5647 (1999).
26. G. W. Sachse, G. F. Hill, L. O. Wade, M. G. Perry, *J. Geophys. Res.* **92**, 2071 (1987).
27. S. A. Vay *et al.*, *J. Geophys. Res.* **104**, 5663 (1999).
28. H. B. Singh, W. H. Brune, J. H. Crawford, D. J. Jacob, P. B. Russell, *J. Geophys. Res.* **111**, D24501 (2006).
29. R. Sander, *Compilation of Henry's Law Constants for Inorganic and Organic Species of Potential Importance in Environmental Chemistry (Version 3)* (1999); available at www.henrys-law.org.
30. M. J. Prather, D. J. Jacob, *Geophys. Res. Lett.* **24**, 3189 (1997).

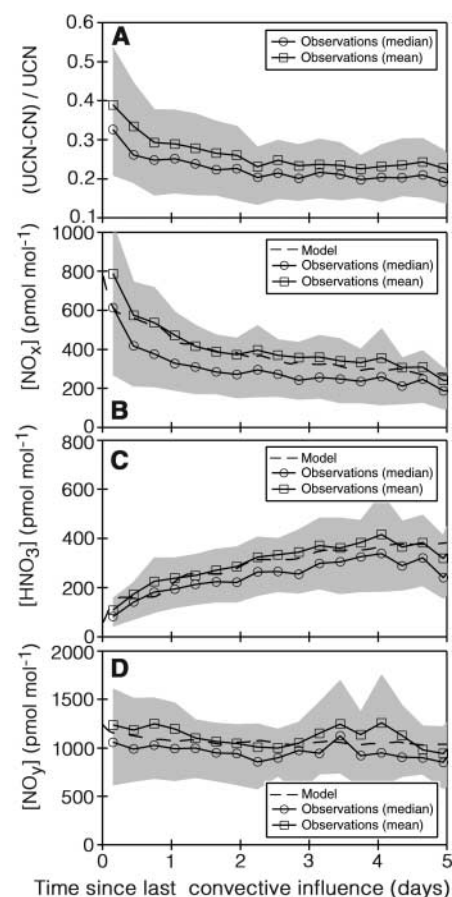


Fig. 4. Observations of (A) the fraction of ultrafine condensation nuclei [number density of aerosol (3 to 10 nm)/total aerosol number density], (B) NO_x , (C) HNO_3 , and (D) NO_y , as a function of modeled time since convective influence. Means and medians of the observations, within 8-hour bins, are shown along with the interquartile range (shaded region). Results from the time-dependent box model, initialized at 10 km and at noon, are shown with dashed lines for the gas-phase species [(B) to (D)].

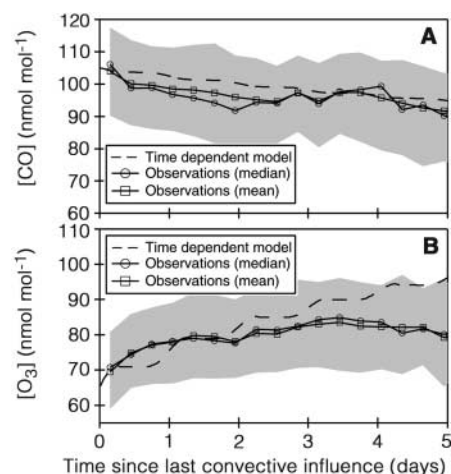
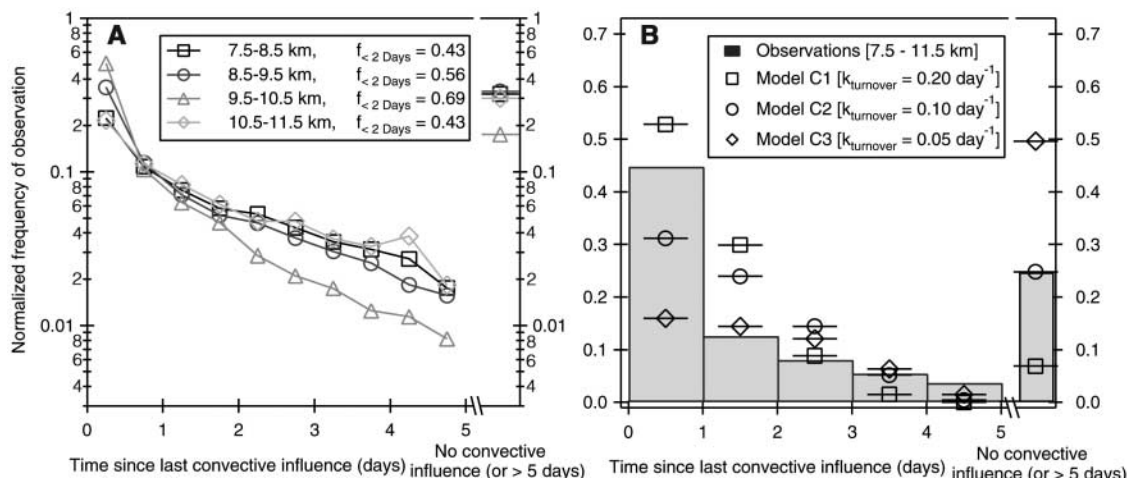


Fig. 5. Observations of CO (A) and ozone (B) as a function of modeled time since cloud processing in the UT. Means and medians of the observations, within 8-hour bins, are shown along with the interquartile range (shaded region). Results from the time-dependent box model, initialized at 10 km and at noon, are shown with dashed lines.

Fig. 6. (A) Normalized frequency distribution in the time since convective influence, as calculated from observations of the NO_x/HNO_3 ratio made during summer 2004. Calculations are separated into 1-km altitude bins (range 7.5 to 11.5 km). The fraction of air that had been influenced by convection within the past 2 days ($f_{<2 \text{ days}}$) is shown. **(B)** Comparison of observed frequency distribution (7.5 to 11.5 km) with various modeled representations of the convective turnover rate.



31. L. Jaeglé *et al.*, *Geophys. Res. Lett.* **25**, 1705 (1998).
32. Y. Wang *et al.*, *Geophys. Res. Lett.* **27**, 369 (2000).
33. D. S. Cohan, M. G. Schultz, D. J. Jacob, B. G. Heikes, D. R. Blake, *J. Geophys. Res.* **104**, 5717 (1999).
34. S. Smyth *et al.*, *J. Geophys. Res.* **101**, 1743 (1996).
35. S. A. McKeen, S. C. Liu, *Geophys. Res. Lett.* **20**, 2363 (1993).
36. F. J. Dentener, P. J. Crutzen, *J. Geophys. Res.* **98**, 7149 (1993).
37. F. Giorgi, W. L. Chameides, *J. Geophys. Res.* **90**, 7872 (1985).
38. D. D. Davis *et al.*, *J. Geophys. Res.* **101**, 2111 (1996).
39. D. J. Jacob *et al.*, *J. Geophys. Res.* **101**, 24235 (1996).
40. R. B. Chatfield, *Geophys. Res. Lett.* **21**, 2705 (1994).
41. A. Tabazadeh *et al.*, *Geophys. Res. Lett.* **25**, 4185 (1998).
42. D. A. Hauglustaine, B. A. Ridley, S. Solomon, P. G. Hess, S. Madronich, *Geophys. Res. Lett.* **23**, 2609 (1996).
43. A. D. Clarke *et al.*, *J. Geophys. Res.* **104**, 5735 (1999).
44. H. Huntrieser *et al.*, *J. Geophys. Res.* **107**, 10.1029/2000JD000209 (2002).
45. See supporting material on Science Online.
46. O. R. Cooper *et al.*, *J. Geophys. Res.* **111**, D24S05 (2006).
47. E. A. Ray *et al.*, *J. Geophys. Res.* **109**, D18304 (2004).
48. T. Hauf, P. Schulte, R. Alheit, H. Schlager, *J. Geophys. Res.* **100**, 22957 (1995).
49. Net ozone concentration change of $0 \text{ nmol mol}^{-1} \text{ day}^{-1}$ could be achieved if the air parcel (i) subsided to where H_2O abundances were large enough to provide a sink of O_3 through O^1D that balanced production from $\text{NO} + \text{HO}_2$ ($\sim 6 \text{ km}$), (ii) entrained air containing lower O_3 mixing ratios, or (iii) contained additional O_3 loss terms beyond NO_x , HO_x , and H_2O (via O^1D removal). To match the deviation between the model and measurement, we would require an additional 2 to $3 \text{ nmol mol}^{-1} \text{ day}^{-1}$ of chemical ozone loss. In order for mixing to explain the deviation, air of lower O_3 would need to be mixed into the air parcel. As shown in Fig. 5B, the only air in the UT containing significantly less O_3 is that which is pumped directly from the PBL. Although mixing fresh and aged outflow could help to explain the discrepancy in O_3 , it is inconsistent with the observed decay in CO at long times (2 to 5 days).
50. D. Rind, J. Lerner, *J. Geophys. Res.* **101**, 12667 (1996).
51. G. L. Mullendore, D. R. Durran, J. R. Holton, *J. Geophys. Res.* **110**, D06113 (2005).
52. K. E. Pickering, Y. S. Wang, W. K. Tao, C. Price, J. F. Muller, *J. Geophys. Res.* **103**, 31203 (1998).
53. W. B. Rossow, <http://isccp.giss.nasa.gov/products/isccpDsets.html> (2006).
54. We used 10-day back-trajectories to National Weather Service Global Forecast System (GFS)-derived convection measurements and NLDN-measured lightning strikes to assess the fraction of time that the DC-8 sampled either convection- or lightning-influenced air. Using the GFS statistics, we calculated that 63% of the sampled air on INTEX-NA had encountered convection and $\sim 57\%$ had been influenced by lightning during the past 2 days. When considering the entire INTEX-NA sampling domain (both in

space and time), convection was present in 12.5% of the grid points. This is substantially smaller than the percentage of observations within 6 hours of convection (21.4%), which suggests that the DC-8 had a positive bias toward sampling fresh convection. This bias is reflected in the sharp drop in population between day 1 and day 2 (Fig. 6A). Correcting for this bias had little effect on our assessment of the fraction of air less than 2 days old, lowering our results from 0.43, 0.56, 0.69, and 0.43 to 0.38, 0.50, 0.62, and 0.39 at 8, 9, 10, and 11 km, respectively.

55. We thank the flight and ground crews of the NASA DC-8 aircraft and the entire INTEX-NA science team for their contributions during the 2004 intensive field campaign; A. M. Thompson, I. Folkins, M. G. Lawrence, and D. Allen for helpful discussions; T. Kucsera for help with the GEOS-4 calculations; and W. H. Brune and X. Ren for OH and HO_2 data. NLDN data were collected by Vaisala-

Thunderstorm and provided to the INTEX Science Team by the Global Hydrology Resource Center at NASA Marshall Space Flight Center. Work at UC Berkeley was supported by NASA grants NNG05GH196 and NAG5-13668. The INTEX-NA field program was supported by the NASA-ESE Tropospheric Chemistry Program.

Supporting Online Material

www.sciencemag.org/cgi/content/full/1134548/DC1
Materials and Methods

Figs. S1 to S8

Table S1

References

31 August 2006; accepted 19 December 2006

Published online 4 January 2007;

10.1126/science.1134548

Include this information when citing this paper.